

HD3C: EFFICIENT MEDICAL DATA CLASSIFICATION FOR EMBEDDED DEVICES

Jianglan Wei^{1,2*}, Zhenyu Zhang^{1*}, Pengcheng Wang^{2*}, Mingjie Zeng¹, and Zhigang Zeng¹

¹ Huazhong University of Science and Technology, Hubei, China

² University of California, Berkeley, CA, USA

ABSTRACT

Energy-efficient medical data classification is essential for modern disease screening, particularly in home and field healthcare where embedded devices are prevalent. While deep learning models achieve state-of-the-art accuracy, their substantial energy consumption and reliance on GPUs limit deployment on such platforms. We present Hyperdimensional Computing with Class-Wise Clustering (HD3C), a lightweight classification framework designed for low-power environments. HD3C encodes data into high-dimensional hypervectors, aggregates them into multiple cluster-specific prototypes, and performs classification through similarity search in hyperspace. We evaluate HD3C across three medical classification tasks; on heart sound classification, HD3C is $350\times$ more energy-efficient than Bayesian ResNet with less than 1% accuracy difference. Moreover, HD3C demonstrates exceptional robustness to noise, limited training data, and hardware error, supported by both theoretical analysis and empirical results, highlighting its potential for reliable deployment in real-world settings. Code is available [here](#).

1 INTRODUCTION

Medical data classification enables automated disease screening without constant involvement of medical professionals (Tan et al., 2024). With the growing adoption of portable devices, health assessments are increasingly carried out in home and field settings where computational resources and power budgets are limited (Rahman & Morshed, 2025). This highlights the need for classification models that can operate effectively on embedded platforms (Khan et al., 2022).

Deep learning models currently dominate medical classification tasks and achieve state-of-the-art accuracy, but their high energy consumption and reliance on GPUs limit deployment on low-power, near-sensor hardware (Chen et al., 2021). In contrast, an optimal medical classifier for embedded devices should: (1) minimize energy consumption, (2) support GPU-free inference, and (3) process data locally to preserve patient privacy.

To address these challenges, we present Hyperdimensional Computing with Class-Wise Clustering (HD3C), a lightweight classification framework that extends the standard Hyperdimensional Computing (HDC). HD3C encodes each sample into a high-dimensional sample hypervector (Sample-HV), aggregates them into a compact set of cluster prototypes (Cluster-HVs), and performs classification by selecting the Cluster-HV with the highest similarity.

Evaluated across three medical classification tasks, HD3C consumes substantially less energy than deep learning baselines while achieving significant accuracy gains over standard HDC. On heart sounds classification, HD3C is $350\times$ more energy-efficient per inference than the state-of-the-art Bayesian ResNet, while providing $>10\%$ accuracy improvement over standard HDC (Figure 1). HD3C also demonstrates exceptional robustness: accuracy drops by only 1.39% under 15% input noise, 1.78% with 40% training data, and 2.84% with 20% parameter corruption (Figure 4). We provide theoretical analysis explaining this robustness, supporting HD3C’s reliability for real-world deployment. Our main contributions are:

* Equal Contribution.

Under review as a conference paper. Please do not distribute.

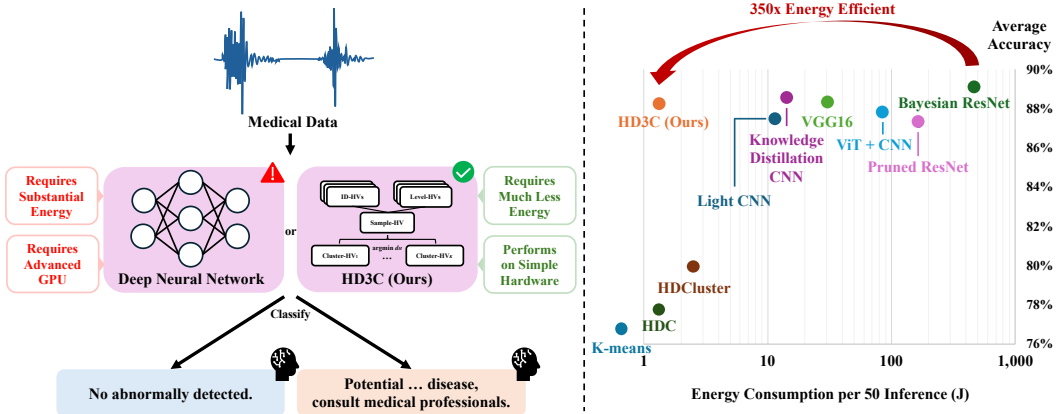


Figure 1: Automated disease screening through medical data classification (left) and HD3C performance on heart sound classification (right). HD3C is 350 \times more energy-efficient than Bayesian ResNet and supports GPU-free inference, highlighting its potential for embedded deployment.

- We propose HD3C, a lightweight classification framework extended from Hyperdimensional Computing (HDC). It achieves significantly higher accuracy than standard HDC and other efficient models while preserving energy efficiency.
- We demonstrate that HD3C achieves substantially lower energy consumption than deep learning baselines across three medical tasks. On heart sound classification, it is 350 \times more energy-efficient than Bayesian ResNet while maintaining comparable accuracy.
- We provide both theoretical and empirical evidence of HD3C’s robustness on input noise and hardware error. To the best of our knowledge, our theorems on binary hypervectors, although some are widely recognized, have not been formally proven in prior HDC research.

This paper is organized as follows. Section 2 reviews the fundamentals of hyperdimensional computing. Section 3 details the proposed HD3C framework. Section 4 presents experimental results and sensitivity analysis, and Section 5 concludes the paper.

2 HYPERDIMENSIONAL COMPUTING (HDC)

Hyperdimensional Computing is a computational paradigm inspired by the information processing mechanisms of the brain (Pentti Kanerva, 2009). Compared with traditional computing that operates on raw numerical data, the human brain processes information via high-dimensional patterns of neural activity (Masse et al., 2009). HDC emulates this approach by projecting input data into high-dimensional representations to efficiently perform cognitive tasks (Thomas et al., 2021).

The versatility of HDC has been demonstrated across a wide array of domains, including image classification (Billmeyer & Parhi, 2021), language identification (Alonso et al., 2021), acoustic signal analysis (Imani et al., 2017), and fault detection (Kleyko et al., 2018). Across these applications, HDC demonstrates superior energy efficiency and robustness compared to deep neural networks.

Specifically, HDC defines a set of elementary operations, like Binding (e.g., point-wise multiplication) and Bundling (e.g., point-wise addition with majority function), on a high-dimensional bipolar vector space $\mathcal{H}^D = \{-1, +1\}^D$ called hyperspace (Pentti Kanerva, 2009). The space is equipped with a distance measure called Hamming distance $d_H : \mathcal{H}^D \times \mathcal{H}^D \rightarrow [0, 1]$, which is defined as the ratio of the different bits between two hypervectors (i.e., hyperspace vectors). Please refer to Appendix A.1 for the detailed notations and definitions.

HDC exhibits several ideal properties when its dimensionality D is very large. For example, the Hamming distance of two hypervectors remains unchanged after bound to the same hypervector (Lemma 2); or when randomly selecting two hypervectors, their Hamming distance is almost always around 0.5 (Lemma 3). Based on these properties, HDC can encode a low-dimensional input

$s \in \mathbb{R}^d (d \ll D)$ from a continuous feature space into the high-dimensional hyperspace. By transferring the calculation to hyperspace, HDC-based approaches can achieve computational efficiency (Ge & Parhi, 2020), robustness to input noise (Thomas et al., 2021), and higher training data efficiency (Asgarinejad et al., 2020).

3 MEDICAL DATA CLASSIFICATION THROUGH HD3C

We propose Hyperdimensional Computing with Class-Wise Clustering (HD3C), an extension of the HDC framework that improves accuracy while preserving energy efficiency. Algorithm 1 and Figure 3 illustrate the overall HD3C pipeline. In this work, medical samples are first encoded into sample hypervectors (Section 3.1). These sample hypervectors are then clustered into a compact set of cluster prototypes, and classification is performed by similarity search against these prototypes (Section 3.2). An optional retraining stage may further enhance accuracy (Section 3.3). Formal definitions, lemma, and theorems supporting this framework are provided in Appendix A.

3.1 ENCODE SAMPLE INTO HYPERVECTOR

HD3C requires numeric features as input. For heart sound classification, we extract $d = 720$ features using Mel-frequency Cepstral Coefficients (MFCC) (Davis & Mermelstein, 1980) and Discrete Wavelet Transform (DWT) (Mallat, 1989), two widely used frequency-domain representations in audio analysis. For breast cancer classification, we use $d = 30$ features from fine-needle aspirate (FNA) breast mass images, and for EMG classification, we use $d = 8$ features.

Each sample’s feature vector $s \in \mathbb{R}^d$ is encoded into a high-dimensional binary hypervector called Sample Hypervector (Sample-HV): $S \in \mathcal{H}^D = \{-1, +1\}^D$, $d \ll D$. The encoder is designed to be continuous so that relative distances between samples are preserved. The first step of encoding divides each feature’s value range into M intervals: the middle 96% of values are split into M equal-width intervals, while the top and bottom 2% are directly mapped to the first and last intervals (Figure 2). This is formalized by function l in Definition 5.

Each interval in Figure 2 is represented by a predefined Level Hypervector (Level-HV), denoted as $L^{(m)} \in \mathcal{H}^D$, $m \in \{1, 2, \dots, M\}$. The Level-HVs are generated in a way that neighboring Level-HVs have a low Hamming distance (i.e. low percentage of different bits): starting from a randomly generated $L^{(1)}$, each subsequent Level-HV is formed by randomly flipping $D/(M-1)$ bits from the previous vector, with each bit flipped only once across the sequence (Definition 4). This ensures that the Hamming distance between any two Level-HVs satisfies:

$$d_H(L^{(i)}, L^{(j)}) = \frac{|i - j|}{M-1}. \quad (1)$$

The Level-HVs are shared across all features. To distinguish identical Level-HVs under different features, each feature is assigned a randomly sampled Identity Hypervector (ID-HV), denoted as $ID^{(n)} \in \mathcal{H}^D$, $n \in \{1, 2, \dots, d\}$. A value in interval I_m under feature n would be represented as $ID^{(n)} \otimes L^{(m)}$, where \otimes denotes the binding operation implemented by point-wise multiplication (Definition 2). Since ID-HVs are randomly sampled, their pairwise Hamming distance is approximately 0.5 (Lemma 3), ensuring feature-wise independence: Hamming distance between two Level-HVs remains unchanged after binding to the same ID-HV (Lemma 2), while those bound to different ID-HVs become effectively unrelated.

Finally, with the predefined Level-HVs and ID-HVs, the encoder maps each medical sample to a Sample-HV by bundling the representations of each feature:

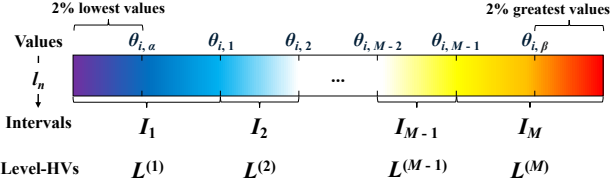


Figure 2: Divide feature n ’s value range into M intervals.

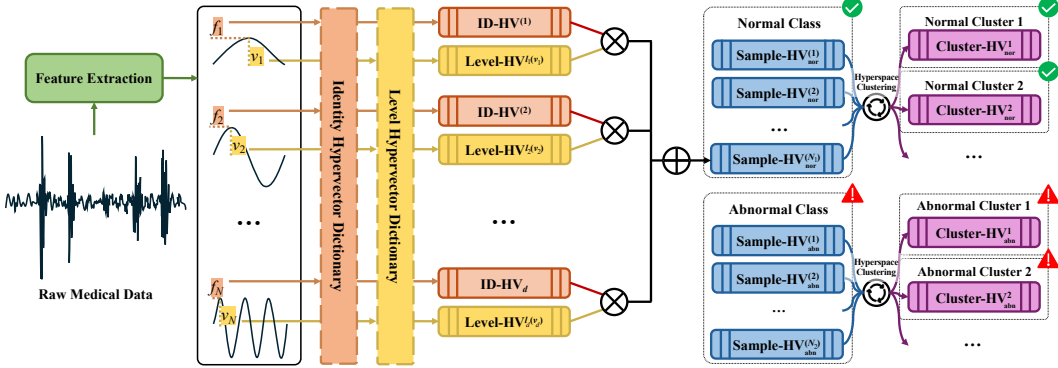


Figure 3: Medical data classification through HD3C: Training samples are encoded into sample hypervectors (Sample-HVs) and aggregated into a compact set of cluster prototypes (Cluster-HVs); new samples are classified by selecting the Cluster-HV with highest similarity. The figure illustrates a binary classification example, though HD3C is not limited to binary tasks.

$$S^{(i)} = \left[\sum_{n=1}^d ID^{(n)} \otimes L^{(l_n(s_n^{(i)}))} \right], \quad (2)$$

where $s_n^{(i)}$ denotes the value of the n^{th} feature in sample $s^{(i)}$, and $[\cdot]$ is the element-wise majority function: it outputs $+1$ for positive sum, -1 for negative sum, and equally random samples from $\{-1, +1\}$ for zero sum (Definition 2).

We demonstrate the inherent robustness of this encoding to input noise through Theorem 1. When noise is applied to a feature vector $s^{(1)}$, producing a perturbed version $s^{(2)}$, the theorem shows that as long as the noise is bounded by a relative ratio δ , the Hamming distance between the corresponding Sample-HVs $S^{(1)}$ and $S^{(2)}$ has an upper bound. This upper bound, expressed as $g(\delta)$, remains quantitatively small even under moderate noise. The formal proof and definition of $g(\delta)$ are provided in Proof 1

Theorem 1 (Robustness to Input Noise). *Let $s^{(1)}, s^{(2)} \in \mathcal{S} \subseteq \mathbb{R}^d$ be two feature vectors. $S = f_{\mathcal{ID}, \mathcal{L}, \Theta}(s)$ denotes the hypervector encoding defined in Equation 2. Suppose that for all indices of the features $n \in \{1, \dots, d\}$,*

$$\frac{|x_n^{(1)} - x_n^{(2)}|}{\Delta_i} \leq \delta, \quad (3)$$

where Δ_i is the difference between the upper and lower bounds of the i^{th} feature value, and $\delta \in [0, 1]$ denotes the maximum distance ratio of the corresponding features. Then, with a sufficiently large D , the expected upper-bound Hamming distance between $S^{(1)} = f_{\mathcal{ID}, \mathcal{L}, \Theta}(s^{(1)})$ and $S^{(2)} = f_{\mathcal{ID}, \mathcal{L}, \Theta}(s^{(2)})$ converges to a monotonically increasing function g with parameter δ :

$$\mathbb{E} \left[\sup \left(d_H \left(S^{(1)}, S^{(2)} \right) \right) \right] \rightarrow g(\delta). \quad (4)$$

This implies that the Hamming distance between a sample and its noisy variant is almost surely bounded by $g(\delta)$.

3.2 CLASS-WISE HYPERSPACE CLUSTERING

Medical data often exhibit substantial intra-class variability beyond simple class labels. For example, heart sounds sharing the same ‘abnormal’ label can differ due to the type and stage of cardiac disease, the stethoscope used, and the recording site on the body (Zipes et al., 2019). Such heterogeneity challenges the standard HDC pipeline, which rely on a single prototype to represent all samples within one class.

Algorithm 1 HD3C: Hyperdimensional Computing with Class-Wise Clustering

```

1:  $\{ID^{(n)}\}_{n=1}^d \leftarrow \text{identity\_hypervectors}(d)$  ▷ Generate ID-HV Dictionary.
2:  $\{L^{(m)}\}_{m=1}^M \leftarrow \text{level\_hypervectors}(M)$  ▷ Generate Level-HV Dictionary.
3: for  $s^{(i)} \in S$  in training set do
4:    $S^{(i)} \leftarrow [\sum_{n=1}^d ID^{(n)} \otimes L^{(l_n(s^{(i)}))}]$  ▷ Encode sample  $s^{(i)}$  into Sample-HV  $S^{(i)}$ .
5: end for
6: for  $j = 1$  to number of classes  $J$  do
7:   for  $S_j^{(i)} \in$  class  $j$  do
8:      $\text{init\_cluster\_idx} \leftarrow \text{randint}(K)$  ▷ Random assign  $S_j^{(i)}$  to one of  $K$  clusters.
9:      $\mathfrak{C}_j^{\text{init\_cluster\_idx}} \leftarrow \mathfrak{C}_j^{\text{init\_cluster\_idx}} \cup \{S_j^{(i)}\}$ 
10:  end for
11: for  $t = 1$  to number of clustering iterations  $T$  do
12:   for  $k = 1$  to number of clusters  $K$  do
13:      $C_j^k \leftarrow [\sum_{S_j^{(i)} \in \mathfrak{C}_j^k} S_j^{(i)}]$  ▷ Generate Cluster-HV  $C_j^k$  to represent cluster  $\mathfrak{C}_j^k$ .
14:   end for
15:   for  $S_j^{(i)} \in$  class  $j$  do
16:      $\text{cluster\_idx} \leftarrow \text{argmin}_{k=1}^K d_H(S_j^{(i)}, C_j^k)$  ▷ Reassign  $S_j^{(i)}$  to closest cluster.
17:      $\mathfrak{C}_j^{\text{cluster\_idx}} \leftarrow \mathfrak{C}_j^{\text{cluster\_idx}} \cup \{S_j^{(i)}\}$ 
18:   end for
19: end for
20: end for
21:  $(\text{class\_idx}, \text{cluster\_idx}) \leftarrow \text{argmin}_{(j,k) \in [J] \times [K]} d_H(S_j^{\text{new}}, C_j^k)$  ▷ Classify new sample.
22: return  $\text{class\_idx}$ 

```

To address this, HD3C introduces class-wise hyperspace clustering. The clustering process is inspired by K-means, but performed in hyperspace on Sample-HVs and applied independently within each class. Unlike K-means which computes arithmetic means, HD3C uses the bundling operation (Definition 2) to form cluster prototypes (Cluster-HVs). Leveraging hypervectors rather than raw numeric features provides the robustness formalized in Theorem 1.

Specifically, for each class j , clustering begins by randomly assigning its Sample-HVs $\{S_j^{(i)}\}$ to K clusters $\{\mathfrak{C}_j^k\}_{k=1}^K$. Each Cluster-HV $C_j^k \in \mathcal{H}^D$ is computed by bundling the Sample-HVs in that cluster:

$$C_j^k = [\sum_{S_j^{(i)} \in \mathfrak{C}_j^k} S_j^{(i)}]. \quad (5)$$

Next, the Sample-HVs are reassigned to the cluster whose prototype has the lowest Hamming distance:

$$S_j^{(i)} \rightarrow \underset{k \in [K]}{\text{argmin}} d_H(S_j^{(i)}, C_j^k), \quad [K] := \{1, 2, \dots, K\}. \quad (6)$$

This bundling and reassigning process is repeated for T iterations until convergence, yielding the final set of Cluster-HVs $\{C_j^k\}_{k=1}^K$ for class j . After clustering all J classes, HD3C may classify an unseen new sample by encoding it as Sample-HV S^{new} and assigning it to the Cluster-HV with the highest similarity (i.e., lowest Hamming distance):

$$S^{\text{new}} \rightarrow \underset{(j,k) \in [J] \times [K]}{\text{argmin}} d_H(S^{\text{new}}, C_j^k). \quad (7)$$

The sample is then classified according to the class label of the selected cluster.

Theorem 2 provides theoretical insight into our clustering-by-bundling method in Equation 5 (Proof 2). It shows that the Hamming distance between the Cluster-HV C and any Sample-HV that constitutes the cluster is almost always less than the typical distance of $d_H = 0.5$ between two random hypervectors. This supports that the Cluster-HV can sufficiently represent all samples in the cluster. Moreover, since Sample-HVs within a cluster are typically more similar to one another than two randomly drawn hypervectors, the Cluster-HV is expected to preserve even stronger relationships in practice than those guaranteed under the random hypervector assumption in the theorem.

Theorem 2 (Distance Between Cluster Prototype and Constituents). *Let $S^{(1)}, S^{(2)}, \dots, S^{(N)} \in \mathcal{H}^D$ be independently sampled random hypervectors. Define their bundling sum as $C = [S^{(1)} + S^{(2)} + \dots + S^{(N)}]$. As $D \rightarrow \infty$, for any random hypervector $S^* \in \mathcal{H}^D$, index $j \in \{1, \dots, N\}$, the Hamming distance between C and any component $S^{(n)}$ satisfies*

$$P \left(d_H(C, S^{(n)}) < d_H(C, S^*) \right) \rightarrow 1. \quad (8)$$

3.3 RETRAIN CLUSTER PROTOTYPES

To further improve accuracy, HD3C optionally applies a retraining procedure that adjusts Cluster-HVs based on misclassified training samples. The retraining stage operates exclusively on the training set with no reference to test data.

Recall that each Cluster-HV C_j^k is generated by bundling the Sample-HVs assigned to cluster \mathfrak{C}_j^k , i.e., $C_j^k = [\sum_{S_j^{(i)} \in \mathfrak{C}_j^k} S_j^{(i)}]$. Let S^{err} be a misclassified Sample-HV from the training set. Suppose $S^{\text{err}} \in \mathfrak{C}_{j_1}^{k_1}$, but its nearest Cluster-HV in Hamming distance is a different Cluster-HV $C_{j_2}^{k_2}$. This implies that the Cluster-HV $C_{j_1}^{k_1}$, constructed from cluster $\mathfrak{C}_{j_1}^{k_1}$, does not adequately represent S^{err} .

To correct this, HD3C performs two adjustments: (1) Subtracts S^{err} from the incorrect Cluster-HV $C_{j_2}^{k_2}$ and (2) Re-bundles S^{err} onto the correct Cluster-HV $C_{j_1}^{k_1}$. We generalize this operation across all misclassified training samples. Let $\mathcal{E}_j^{\text{k,out}}$ denote Sample-HVs outside cluster \mathfrak{C}_j^k that incorrectly match closest to C_j^k ; while $\mathcal{E}_j^{\text{k,in}}$ denote the Sample-HVs within \mathfrak{C}_j^k but are closer to a Cluster-HV of a different cluster. The retrained Cluster-HV representing cluster \mathfrak{C}_j^k is computed as

$$C_j^{k'} = \left[\sum_{S_j^{(i)} \in \mathfrak{C}_j^k} S_j^{(i)} - \sum_{S_j^{(i)} \in \mathcal{E}_j^{\text{k,out}}} S_j^{(i)} + \sum_{S_j^{(i)} \in \mathcal{E}_j^{\text{k,in}}} S_j^{(i)} \right]. \quad (9)$$

4 RESULTS AND DISCUSSIONS

4.1 DATASETS

PhysioNet/CinC Challenge 2016 (Clifford et al., 2016) provides a collection of 3,153 heart sound recordings sourced from six distinct databases. These recordings were collected by multiple research teams across various countries using different equipment and methodologies, often under noisy conditions. Each recording is labeled as either ‘normal’ or ‘abnormal’.

Wisconsin Breast Cancer (William Wolberg et al., 1995) is a widely used benchmark for breast cancer diagnosis. It contains real-valued features extracted from digitized images of fine-needle aspirates (FNA) of breast masses, with each sample labeled as either ‘benign’ or ‘malignant’.

Cerqueira sEMG Muscle Fatigue (Cerqueira et al., 2024) offers surface electromyography (sEMG) recordings using a Delsys Trigno system at a sampling frequency of 1259Hz. Each sample is annotated into three fatigue levels: relax, mild fatigue, and fatigued.

4.2 EXPERIMENT SETUP

Platform: Large deep learning baselines were trained and evaluated on an NVIDIA GeForce RTX 4090 GPU (24GB VRAM). HD3C, other one-shot models, and efficient neural networks were

Table 1: Performance and Energy Comparison of HD3C and Baseline Models

Models	10-Folds Accuracy (%)	Energy (Train, J)	Energy (1000 Inferences, J)
PhysioNet Challenge 2016:			
Bayesian ResNet (H. Krones et al., 2022)	89.105 \pm 1.543	142997 \pm 5465	9455 \pm 899
Knowledge Distillation CNN (Song et al., 2023)	88.580 \pm 2.186	32808 \pm 2582	289 \pm 116
VGG16 (Shuvo et al., 2023)	88.271 \pm 1.718	165840 \pm 5443	605 \pm 131
ViT + CNN (Han & Shaout, 2025)	87.808 \pm 1.996	889920 \pm 36748	1661 \pm 209
Light CNN (Li et al., 2021)	87.408 \pm 1.497	10164 \pm 1204	227 \pm 88
Pruned Bayesian ResNet (H. Krones et al., 2022)	87.190 \pm 2.508	142997 \pm 5465	3307 \pm 214
Class-Wise K-Means	76.759 \pm 4.937	9 \pm 2	very low
HDCluster (Imani et al., 2019)	79.877 \pm 2.589	318 \pm 3	50 \pm 2
HDC	77.840 \pm 2.419	135 \pm 10	26 \pm 4
HD3C (Ours)	88.180 \pm 1.746	246 \pm 6	27 \pm 3
Wisconsin Breast Cancer:			
DNN (Zheng, 2024)	96.842 \pm 2.579	698.626 \pm 82.403	11.842 \pm 1.470
GRU (Jony & Arnob, 2024)	96.668 \pm 1.994	2710.461 \pm 109.069	97.283 \pm 2.408
CNN (Jony & Arnob, 2024)	95.439 \pm 2.956	312.416 \pm 7.874	12.458 \pm 0.368
Class-Wise K-Means	93.595 \pm 3.106	3.045 \pm 0.379	0.070 \pm 0.007
HDC	94.382 \pm 0.039	2.489 \pm 0.174	0.717 \pm 0.021
HD3C (Ours)	96.314 \pm 0.027	3.801 \pm 0.340	0.823 \pm 0.015
Cerveira sEMG Muscle Fatigue:			
GRU (Aviles et al., 2024)	91.955 \pm 3.084	874.511 \pm 42.378	34.018 \pm 1.013
LSTM (Aviles et al., 2024)	91.710 \pm 2.705	135.828 \pm 7.453	32.416 \pm 1.483
CNN (Moniri et al., 2021)	91.367 \pm 3.626	250.685 \pm 21.217	10.426 \pm 0.884
Class-Wise K-Means	88.596 \pm 5.135	3.367 \pm 0.247	0.076 \pm 0.010
HDC (Moin et al., 2018)	84.984 \pm 0.043	2.634 \pm 0.169	0.445 \pm 0.025
HD3C (Ours)	91.592 \pm 2.927	2.813 \pm 0.205	0.422 \pm 0.029

trained and evaluated on an Intel Xeon Gold 6430 CPU (120GB RAM). All experiments were conducted on Ubuntu 22.04.1 LTS (Linux kernel 5.15.0-97-generic).

Energy Measurement: We define *energy* as device-level energy consumption (joules). Training and inference energy were computed by integrating measured power over time.

4.3 COMPARISON WITH BASELINE MODELS

Table 1 summarizes the performance of HD3C against baseline models across three medical datasets. HD3C achieves substantially higher energy efficiency than deep neural networks and outperforms other efficient methods in terms of accuracy. For instance, on the heart sounds classification task, HD3C is 580 \times more energy-efficient in training and 350 \times in inference compared to the best-performing Bayesian ResNet (H. Krones et al., 2022), while also delivering a 10% accuracy improvement over standard HDC.

4.4 IMPACT OF HD3C HYPERPARAMETERS

As discussed in Section 3, a sufficiently large dimensionality D is critical for HD3C to maintain robustness against input noise (Theorem 1) and to ensure that Cluster-HVs accurately capture the aggregate features of their clusters (Theorem 2). Likewise, an adequate number of clusters K are essential for forming stable hyperspace clusters. A few retrain epochs can further fine-tune Cluster-HVs to better align with the Sample-HVs assigned to each cluster.

However, excessively large values of these hyperparameters introduce unnecessary computational overhead, reducing the energy efficiency HD3C is designed to achieve. Our experiments also indicate that allocating too many clusters or performing excessive retraining can lead to overfitting. Figure 4 (a-c) illustrates HD3C’s performance on heart sound classification across different hyperparameter settings.

4.5 ROBUSTNESS FOR REAL-WORLD DEPLOYMENT

4.5.1 RESILIENCE TO INPUT NOISE

Real-world medical signals often contain persistent environmental noise, which can impair classification performance (Clifford et al., 2016). The inherent robustness of HD3C’s encoding mechanism,

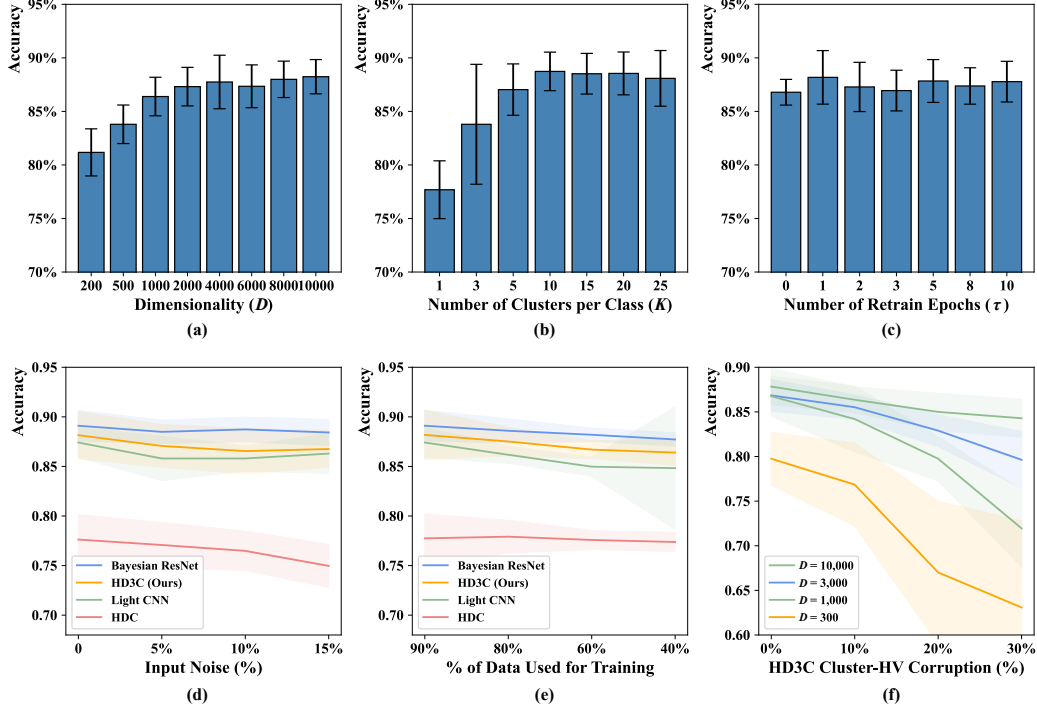


Figure 4: HD3C sensitivity to hyperparameters, input noise, limited training data, and hardware errors on PhysioNet 2016.

as supported by Theorem 1, allows it to maintain high accuracy even with noisy inputs. As shown in Figure 4(d), HD3C experiences only 1.39% drop in accuracy under 15% input noise, demonstrating its reliability in noisy settings.

4.5.2 RESILIENCE TO LIMITED TRAINING DATA

Many medical datasets are limited in size due to privacy constraints. As shown in Figure 4(e), HD3C remains robust under reduced training data, with only a 1.78% drop in accuracy when trained on 40% of the PhysioNet 2016 dataset.

4.5.3 RESILIENCE TO HARDWARE ERRORS

Neural architectures are known for their fault tolerance through redundant representations, unlike traditional binary systems where single-bit failures are critical (Pentti Kanerva, 2009). Similarly, brain-inspired hyperdimensional encodings offer inherent robustness to hardware malfunctions by distributing information across high-dimensional vectors (Kanerva et al., 2000).

To evaluate this robustness in HD3C, we conducted a perturbation analysis by randomly flipping elements (+1 to -1 and vice versa) in all stored Cluster-HVs to simulate hardware instability. Theorem 3 demonstrates that, with sufficient dimensionality, flipping up to 50% of the elements has minimal impact on classification accuracy (Proof 3). The theorem is supported empirically: as shown in Figure 4(f), with $D = 10,000$, flipping 20% of elements results in only a 2.84% drop in accuracy.

Theorem 3 (Robustness to Hardware Error). *Assume we have a Sample-HV S and two Cluster-HVs C_1 and C_2 , whose initial Hamming distances satisfy:*

$$d_H(S, C_1) = d_1 \quad \text{and} \quad d_H(S, C_2) = d_2, \quad (10)$$

where $d_2 - d_1 = \epsilon > 0$.

We randomly flip a proportion p ($p < 0.5$) of the bits in both C_1 and C_2 , yielding two new hyper-vectors C'_1 and C'_2 . As $D \rightarrow \infty$, we have

$$P(d_H(S, C'_1) < d_H(S, C'_2)) \rightarrow 1 \quad (11)$$

4.6 CONCEPTUAL HARDWARE FRAMEWORK

The current implementation of HD3C is in Python, which does not fully exploit the hardware-level efficiency of binary hypervectors enabled by single-bit operations and parallel computing. Prior work on HDC hardware has shown that fundamental operations such as binding and bundling can be implemented with extremely lightweight digital logic: binding reduces to bitwise XOR, bundling to majority voting circuits, and similarity search to parallelized Hamming distance computation (Imani et al., 2017). These properties allow HDC systems to operate with low energy consumption and high throughput compared to conventional floating-point ML models.

Building on these insights, we outline a conceptual hardware framework specifically tailored for HD3C (Figure 5). To validate its feasibility, we prototyped the framework on a Xilinx FPGA platform and are able to achieve the accuracy reported in Table 1. We plan to further refine and evaluate this hardware-oriented design in future work.

5 CONCLUSION

This paper introduces HD3C, an energy-efficient classification framework extended from Hyperdimensional Computing (HDC). HD3C demonstrates significant advantage in medical data classification: on heart sound classification, it is $350\times$ more efficient than Bayesian ResNet, and provide $> 10\%$ accuracy improvement over standard HDC.

We evaluated HD3C’s robustness both theoretically and empirically. The model maintains high accuracy under challenging conditions: showing only a 1.39% drop under 15% input noise, 1.78% when trained on just 40% of the dataset, and 2.84% when 20% of its learned parameters are corrupted. These results highlight HD3C’s reliability on real-world medical applications.

From a societal perspective, HD3C can help expand access to medical screening in underserved settings by enabling assessments on low-cost, GPU-free devices. However, overreliance on the screening tool without clinical oversight could lead to misdiagnoses; therefore, the system should be designed to recommend follow-up with a medical professional when abnormalities are detected.

REPRODUCIBILITY STATEMENT

We are committed to ensuring the reproducibility of our results. To this end, we have released the complete HD3C codebase along with a detailed installation guide in the Supplementary Materials. The repository contains all datasets used in our experiments as well as the exact hyperparameter configurations adopted for training and evaluation. This enables researchers to fully replicate our experiments and verify the reported results.

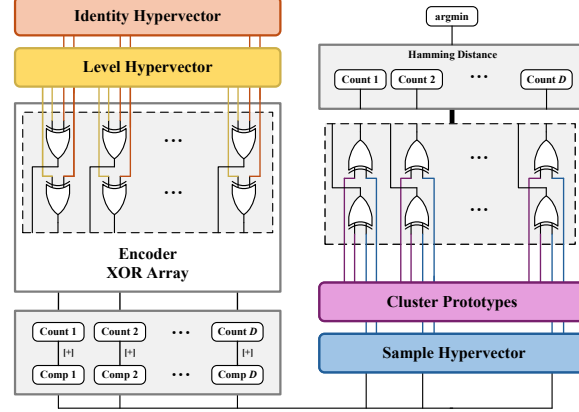


Figure 5: Conceptual hardware framework for HD3C.

REFERENCES

Pedro Alonso, Kumar Shridhar, Denis Kleyko, Evgeny Osipov, and Marcus Liwicki. HyperEmbed: Tradeoffs Between Resources and Performance in NLP Tasks with Hyperdimensional Computing Enabled Embedding of n-gram Statistics. In *2021 International Joint Conference on Neural Networks (IJCNN)*, pp. 1–9, Shenzhen, China, July 2021. IEEE. ISBN 978-1-66543-900-8. doi: 10.1109/IJCNN52387.2021.9534359. URL <https://ieeexplore.ieee.org/document/9534359/>.

Fatemeh Asgarinejad, Anthony Thomas, and Tajana Rosing. Detection of Epileptic Seizures from Surface EEG Using Hyperdimensional Computing. In *2020 42nd Annual International Conference of the IEEE Engineering in Medicine & Biology Society (EMBC)*, pp. 536–540, July 2020. doi: 10.1109/EMBC44109.2020.9175328. URL <https://ieeexplore.ieee.org/document/9175328/?arnumber=9175328>. ISSN: 2694-0604.

Marcos Aviles, José Manuel Alvarez-Alvarado, Jose-Billerman Robles-Ocampo, Perla Yazmín Sevilla-Camacho, and Juvenal Rodríguez-Reséndiz. Optimizing RNNs for EMG Signal Classification: A Novel Strategy Using Grey Wolf Optimization. *Bioengineering*, 11(1):77, January 2024. ISSN 2306-5354. doi: 10.3390/bioengineering11010077. URL <https://www.mdpi.com/2306-5354/11/1/77>.

Ryan Billmeyer and Keshab K. Parhi. Biological Gender Classification from fMRI via Hyperdimensional Computing. In *2021 55th Asilomar Conference on Signals, Systems, and Computers*, pp. 578–582, Pacific Grove, CA, USA, October 2021. IEEE. ISBN 978-1-66545-828-3. doi: 10.1109/IEEECONF53345.2021.9723179. URL <https://ieeexplore.ieee.org/document/9723179/>.

Sara M. Cerqueira, Rita Vilas Boas, Joana Figueiredo, and Cristina P. Santos. A Comprehensive Dataset of Surface Electromyography and Self-Perceived Fatigue Levels for Muscle Fatigue Analysis. *Sensors*, 24(24):8081, December 2024. ISSN 1424-8220. doi: 10.3390/s24248081. URL <https://www.mdpi.com/1424-8220/24/24/8081>.

Yanjiao Chen, Baolin Zheng, Zihan Zhang, Qian Wang, Chao Shen, and Qian Zhang. Deep Learning on Mobile and Embedded Devices: State-of-the-art, Challenges, and Future Directions. *ACM Computing Surveys*, 53(4):1–37, July 2021. ISSN 0360-0300, 1557-7341. doi: 10.1145/3398209. URL <https://dl.acm.org/doi/10.1145/3398209>.

Gari Clifford, Chengyu Liu, David Springer, Benjamin Moody, Qiao Li, Ricardo Abad, Jose Millet, Ikaro Silva, Alistair Johnson, and Roger Mark. Classification of Normal/Abnormal Heart Sound Recordings: the PhysioNet/Computing in Cardiology Challenge 2016. In *2016 Computing in Cardiology Conference*, September 2016. doi: 10.22489/CinC.2016.179-154. URL <http://www.cinc.org/archives/2016/pdf/179-154.pdf>.

S. Davis and P. Mermelstein. Comparison of parametric representations for monosyllabic word recognition in continuously spoken sentences. *IEEE Transactions on Acoustics, Speech, and Signal Processing*, 28(4):357–366, August 1980. ISSN 0096-3518. doi: 10.1109/TASSP.1980.1163420. URL <https://ieeexplore.ieee.org/abstract/document/1163420>.

Lulu Ge and Keshab K. Parhi. Classification Using Hyperdimensional Computing: A Review. *IEEE Circuits and Systems Magazine*, 20(2):30–47, 2020. ISSN 1558-0830. doi: 10.1109/MCAS.2020.2988388. URL <https://ieeexplore.ieee.org/document/9107175/?arnumber=9107175>. Conference Name: IEEE Circuits and Systems Magazine.

”Felix H. Krones, Benjamin Walker, Adam Mahdi, Ivan Kiskin, Terry Lyons, and Guy Parsons”. Dual Bayesian ResNet: A Deep Learning Approach to Heart Murmur Detection. December 2022. doi: 10.22489/CinC.2022.355. URL <https://www.cinc.org/archives/2022/pdf/CinC2022-355.pdf>.

Jiho Han and Adnan Shaout. ENACT-Heart – ENsemble-based Assessment Using CNN and Transformer on Heart Sounds, February 2025. URL <http://arxiv.org/abs/2502.16914> [cs]. arXiv:2502.16914 [cs].

Mohsen Imani, Deqian Kong, Abbas Rahimi, and Tajana Rosing. VoiceHD: Hyperdimensional Computing for Efficient Speech Recognition. In *2017 IEEE International Conference on Rebooting Computing (ICRC)*, pp. 1–8, Washington, DC, November 2017. IEEE. ISBN 978-1-5386-1553-9. doi: 10.1109/ICRC.2017.8123650. URL <http://ieeexplore.ieee.org/document/8123650/>.

Mohsen Imani, Yeseong Kim, Thomas Worley, Saransh Gupta, and Tajana Rosing. HDCluster: An Accurate Clustering Using Brain-Inspired High-Dimensional Computing. In *2019 Design, Automation & Test in Europe Conference & Exhibition (DATE)*, pp. 1591–1594, March 2019. doi: 10.23919/DATE.2019.8715147. URL <https://ieeexplore.ieee.org/document/8715147/?arnumber=8715147>. ISSN: 1558-1101.

Akinul Islam Jony and Arjun Kumar Bose Arnob. Deep Learning Paradigms for Breast Cancer Diagnosis: A Comparative Study on Wisconsin Diagnostic Dataset. *Malaysian Journal of Science and Advanced Technology*, pp. 109–117, March 2024. ISSN 2785-8901. doi: 10.56532/mjsat.v4i2.245. URL <https://mjsat.com.my/index.php/mjsat/article/view/245>.

Pentti Kanerva, Jan Kristoferson, and Anders Holst. Random Indexing of Text Samples for Latent Semantic Analysis. *Proceedings of the 22nd Annual Conference of the Cognitive Science Society*, pp. 1036, 2000.

Firoz Khan, Balusupati Veera Venkata Siva Prasad, Salman Ali Syed, Imran Ashraf, and Lakshmana Kumar Ramasamy. An Efficient, Ensemble-Based Classification Framework for Big Medical Data. *Big Data*, 10(2):151–160, April 2022. ISSN 2167-6461, 2167-647X. doi: 10.1089/big.2021.0132. URL <https://www.liebertpub.com/doi/10.1089/big.2021.0132>.

Denis Kleyko, Evgeny Osipov, Nikolaos Papakonstantinou, and Valeriy Vyatkin. Hyperdimensional Computing in Industrial Systems: The Use-Case of Distributed Fault Isolation in a Power Plant. *IEEE Access*, 6:30766–30777, 2018. ISSN 2169-3536. doi: 10.1109/ACCESS.2018.2840128. URL <https://ieeexplore.ieee.org/document/8367786/>.

Tao Li, Yibo Yin, Kainan Ma, Sitao Zhang, and Ming Liu. Lightweight End-to-End Neural Network Model for Automatic Heart Sound Classification. *Information*, 12(2):54, February 2021. ISSN 2078-2489. doi: 10.3390/info12020054. URL <https://www.mdpi.com/2078-2489/12/2/54>. Number: 2 Publisher: Multidisciplinary Digital Publishing Institute.

S.G. Mallat. A theory for multiresolution signal decomposition: the wavelet representation. *IEEE Transactions on Pattern Analysis and Machine Intelligence*, 11(7):674–693, July 1989. ISSN 1939-3539. doi: 10.1109/34.192463. URL <https://ieeexplore.ieee.org/document/192463>.

Nicolas Y. Masse, Glenn C. Turner, and Gregory S.X.E. Jefferis. Olfactory Information Processing in Drosophila. *Current Biology*, 19(16):R700–R713, August 2009. ISSN 09609822. doi: 10.1016/j.cub.2009.06.026. URL <https://linkinghub.elsevier.com/retrieve/pii/S0960982209013013>.

Ali Moin, Andy Zhou, Abbas Rahimi, Simone Benatti, Alisha Menon, Senam Tamakloe, Jonathan Ting, Natasha Yamamoto, Yasser Khan, Fred Burghardt, Luca Benini, Ana C. Arias, and Jan M. Rabaey. An EMG Gesture Recognition System with Flexible High-Density Sensors and Brain-Inspired High-Dimensional Classifier. In *2018 IEEE International Symposium on Circuits and Systems (ISCAS)*, pp. 1–5, Florence, 2018. IEEE. ISBN 978-1-5386-4881-0. doi: 10.1109/ISCAS.2018.8351613. URL <https://ieeexplore.ieee.org/document/8351613/>.

Ahmad Moniri, Dan Terracina, Jesus Rodriguez-Manzano, Paul H. Strutton, and Pantelis Georgiou. Real-Time Forecasting of sEMG Features for Trunk Muscle Fatigue Using Machine Learning. *IEEE Transactions on Biomedical Engineering*, 68(2):718–727, February 2021. ISSN 0018-9294, 1558-2531. doi: 10.1109/TBME.2020.3012783. URL <https://ieeexplore.ieee.org/document/9152074/>.

Pentti Kanerva. Hyperdimensional Computing: An Introduction to Computing in Distributed Representation with High-Dimensional Random Vectors, January 2009.

Mahfuzur Rahman and Bashir I. Morshed. Resource-Constrained On-Chip AI Classifier for Beat-by-Beat Real-Time Arrhythmia Detection with an ECG Wearable System. *Electronics*, 14(13): 2654, June 2025. ISSN 2079-9292. doi: 10.3390/electronics14132654. URL <https://www.mdpi.com/2079-9292/14/13/2654>.

Samiul Based Shuvo, Syed Samiul Alam, Syeda Umme Ayman, Arbil Chakma, Prabal Datta Barua, and U Rajendra Acharya. NRC-Net: Automated noise robust cardio net for detecting valvular cardiac diseases using optimum transformation method with heart sound signals. *Biomedical Signal Processing and Control*, 86:105272, September 2023. ISSN 1746-8094. doi: 10.1016/j.bspc.2023.105272. URL <https://www.sciencedirect.com/science/article/pii/S174680942300705X>.

Zikai Song, Lixian Zhu, Yiyan Wang, Mengkai Sun, Kun Qian, Bin Hu, Yoshiharu Yamamoto, and Björn W. Schuller. Cutting Weights of Deep Learning Models for Heart Sound Classification: Introducing a Knowledge Distillation Approach. In *2023 45th Annual International Conference of the IEEE Engineering in Medicine & Biology Society (EMBC)*, pp. 1–4, July 2023. doi: 10.1109/EMBC40787.2023.10340704. URL <https://ieeexplore.ieee.org/abstract/document/10340704>. ISSN: 2694-0604.

Si Ying Tan, Jennifer Sumner, Yuchen Wang, and Alexander Wenjun Yip. A systematic review of the impacts of remote patient monitoring (RPM) interventions on safety, adherence, quality-of-life and cost-related outcomes. *npj Digital Medicine*, 7(1):192, July 2024. ISSN 2398-6352. doi: 10.1038/s41746-024-01182-w. URL <https://www.nature.com/articles/s41746-024-01182-w>.

Anthony Thomas, Sanjoy Dasgupta, and Tajana Rosing. A Theoretical Perspective on Hyperdimensional Computing. *Journal of Artificial Intelligence Research*, 72:215–249, October 2021. ISSN 1076-9757. doi: 10.1613/jair.1.12664. URL <https://www.jair.org/index.php/jair/article/view/12664>.

William Wolberg, W. Street, and Olvi Mangasarian. Breast Cancer Wisconsin (Prognostic), 1995.

Lily Zheng. Training Artificial Neural Network for Breast Cancer Detection: a High Accuracy Model to Compare Different Features of Breast Cell Nuclei in Breast Cancer Diagnosis. October 2024.

Douglas P. Zipes, Peter Libby, Robert O. Bonow, Douglas L. Mann, Gordon F. Tomaselli, and Eugene Braunwald (eds.). *Braunwald's heart disease: a textbook of cardiovascular medicine*. Elsevier, Philadelphia, PA, eleventh edition, international edition edition, 2019. ISBN 978-0-323-46342-3 978-0-323-46299-0 978-0-323-55592-0.

A THEORY

A.1 NOTATIONS AND DEFINITIONS

Definition 1 (Hyperspace). *The hyperspace \mathcal{H}^D is the set of all bipolar hypervectors of dimension D , where each element takes a value from $\{+1, -1\}$. Formally,*

$$\mathcal{H}^D := \{-1, +1\}^D = \{A \in \mathbb{R}^D \mid a_i \in \{+1, -1\}, \forall i \in \{1, 2, \dots, D\}\} \quad (12)$$

where a_i denotes the i -th component of the hypervector A .

Unless otherwise specified, for a random hypervector $A \in \mathcal{H}^D$, each component a_i is drawn independently and identically distributed (i.i.d.) from a binary distribution over $\{-1, +1\}$ with equal probability:

$$\mathbb{P}(a_i = +1) = \mathbb{P}(a_i = -1) = 0.5, \quad \forall i \in \{1, \dots, d\}. \quad (13)$$

Definition 2 (Elementary Functions). *Given any hypervectors $A, B \in \mathcal{H}^D$, we define the following elementary functions:*

- The number of $+1$ elements in A :

$$pos(A) := \sum_{i=1}^D \mathbb{I}(a_i = +1) \quad (14)$$

- The number of -1 elements in A :

$$neg(A) := \sum_{i=1}^D \mathbb{I}(a_i = -1) \quad (15)$$

- Binding of A and B :

$$A \otimes B := A \times B \quad (16)$$

- Bundling of A and B :

$$A \oplus B := [A + B] \quad (17)$$

where $\mathbb{I}(\cdot)$ denotes the indicator function that returns 1 if the condition is true and 0 otherwise, \times is an element-wise multiplication, $+$ is an element-wise addition, and $[\cdot]$ is the element-wise majority function that outputs -1 for negative sum, $+1$ for positive sum, and equally random drawn from $\{-1, +1\}$ for zero sum.

Definition 3 (Hamming Distance). Given two hypervectors $A, B \in \mathcal{H}^D$, the Hamming distance between them is defined as the ratio of positions where the corresponding components differ. Formally,

$$d_H : \mathcal{H}^D \times \mathcal{H}^D \rightarrow [0, 1], \quad d_H(A, B) = \frac{1}{D} \sum_{i=1}^D \mathbb{I}(a_i \neq b_i) = \frac{1}{D} neg(A \otimes B). \quad (18)$$

Definition 4 (Level Set). We define a set of M hypervectors $\mathcal{L} = \{L^{(j)}\}_{j \in \{1, 2, \dots, M\}} \subset \mathcal{H}^D$ as a level set if it can be generated by:

- Randomly sample a base hypervector $L^{(1)} \in \mathcal{H}^D$
- Initialize an empty set $\mathcal{B} = \emptyset$ to record flipped bit positions.
- For each $i \in \{2, 3, \dots, M\}$:
 - Randomly select $\frac{D}{M-1}$ positions from $\{1, \dots, D\} \setminus \mathcal{B}$ (i.e., bits not yet flipped). To avoid unnecessary complexity, we assume that $M-1$ divides D exactly here, i.e., $\frac{D}{M-1} \in \mathbb{N}$.
 - Flip the selected bits in $L^{(i-1)}$ to obtain $L^{(i)}$;
 - Update \mathcal{B} to include the newly flipped bit positions.

In the constructed level set \mathcal{L} , the Hamming distance between any two levels $L^{(i)}$ and $L^{(j)}$ satisfies

$$d_H(L^{(i)}, L^{(j)}) = \frac{|i - j|}{M - 1}.$$

Definition 5 (Mapping with Levels). Let $\mathcal{X} \subseteq \mathbb{R}^d$ be a continuous feature vector space. Define independently sampled d random hypervectors $\mathcal{ID} = \{ID^{(1)}, ID^{(2)}, \dots, ID^{(d)}\} \subset \mathcal{H}^D$ and a random level set $\mathcal{L} = \{L^{(1)}, L^{(2)}, \dots, L^{(M)}\} \subset \mathcal{H}^D$. Next, for each feature dimension $n \in \{1, \dots, d\}$, define $M-1$ real-valued thresholds $\theta_{n,1} < \theta_{n,2} < \dots < \theta_{n,M-1}$, partitioning \mathbb{R} into M intervals:

$$I_0 = (-\infty, \theta_{n,1}), \quad I_1 = [\theta_{n,1}, \theta_{n,2}), \quad \dots, \quad I_{M-1} = [\theta_{n,M-1}, +\infty).$$

Based on the intervals defined by $\Theta = \{\theta_{n,m}\}_{n \in \{1, \dots, d\}, m \in \{1, \dots, M\}}$, we select the unique $m = l_n(x_i[n])$ for $x_i[n] \in \mathbb{R}$ that $x_i[n] \in I_m$.

In this task, the mapping function for feature n is defined by

$$l_n(x) = \begin{cases} 1 & x \in (-\infty, \theta_{n,\alpha}) \\ \lfloor \frac{x - \theta_{n,\alpha}}{\theta_{n,\beta} - \theta_{n,\alpha}} \times M + 1 \rfloor & x \in [\theta_{n,\alpha}, \theta_{n,\beta}) \\ M & x \in [\theta_{n,\beta}, \infty) \end{cases},$$

where $\theta_{n,\alpha}$ and $\theta_{n,\beta}$ denote the 2% and 98% quantiles of values in feature n , respectively.

A.2 LEMMAS AND PROPOSITIONS

Lemma 1 (Hamming Distance between product and multiplier). *Given hypervectors $A, B \in \mathcal{H}^D$, the Hamming distance $d_H(A, A * B)$ depends only on B . Specifically,*

$$d_H(A, A * B) = \frac{1}{D} \text{neg}(B). \quad (19)$$

Proof. By the definition of Binding, the i -th element of $A * B$ is $a_i * b_i$, which behaves as:

$$a_i * b_i = \begin{cases} a_i, & \text{if } b_i = +1, \\ -a_i, & \text{if } b_i = -1. \end{cases} \quad \text{or } a_i \neq (a_i * b_i) \iff b_i = -1$$

Therefore,

$$d_H(A, A * B) = \frac{1}{D} \sum_{i=1}^D \mathbb{I}(a_i \neq (a_i * b_i)) = \frac{1}{D} \sum_{i=1}^D \mathbb{I}(b_i = -1) = \frac{1}{D} \text{neg}(B).$$

□

Lemma 2 (Hamming Distance Preservation under Multiplication). *Given hypervectors $A, B, C \in \mathcal{H}^D$, we have*

$$d_H(A * B, B * C) = d_H(A, C). \quad (20)$$

Proof. By the definition of Binding, the i -th elements of $A * B$ and $B * C$ are $a_i * b_i$ and $b_i * c_i$.

Since $b_i \neq 0$, we have $a_i * b_i \neq b_i * c_i \iff a_i \neq c_i$. Therefore,

$$d_H(A * B, B * C) = \frac{1}{D} \sum_{i=1}^D \mathbb{I}(a_i * b_i \neq b_i * c_i) = \frac{1}{D} \sum_{i=1}^D \mathbb{I}(a_i \neq c_i) = d_H(A, C).$$

□

Lemma 3 (Hamming distance between two Random Hypervectors). *Let $A, B \in \mathcal{H}^D$ be two random hypervectors. Then, for any $\epsilon > 0$,*

$$\lim_{D \rightarrow \infty} \mathbb{P}(|d_H(A, B) - 0.5| > \epsilon) = 0. \quad (21)$$

Proof. Define random variables $X_i := \mathbb{I}(a_i \neq b_i)$, where $X_i = 1$ if $a_i \neq b_i$ and $X_i = 0$ otherwise. By definition,

$$d_H(A, B) = \frac{1}{D} \sum_{i=1}^D X_i.$$

Since A and B are random hypervectors, their components a_i and b_i are drawn i.i.d. from a binary distribution over $\{-1, +1\}$ with equal probability. Thererfore,

$$\mathbb{P}(a_i \neq b_i) = 0.5, \quad \mathbb{P}(a_i = b_i) = 0.5,$$

indicating that each X_i is an independent Bernoulli random variable with $\mathbb{E}[X_i] = 0.5$. Furthermore, we know that the average of i.i.d. sequence $\{X_i\}$, $\frac{1}{D} \sum_{i=1}^D X_i$ follows a scaled Binomial distribution:

$$d_H(A, B) = \frac{1}{D} \sum_{i=1}^D X_i \sim \frac{1}{D} \text{Binomial}(D, \frac{1}{2}).$$

Applying the Weak Law of Large Numbers to the i.i.d. sequence $\{X_i\}$, for any $\epsilon > 0$,

$$\lim_{D \rightarrow \infty} \mathbb{P} \left(\left| \frac{1}{D} \sum_{i=1}^D X_i - 0.5 \right| > \epsilon \right) = 0.$$

Thus,

$$\lim_{D \rightarrow \infty} \mathbb{P} (|d_H(A, B) - 0.5| > \epsilon) = 0.$$

□

Lemma 4. Let $A, B \in \mathcal{H}^D$ be two random hypervectors, Then, for any $\epsilon > 0$,

$$\lim_{D \rightarrow \infty} \mathbb{P} (|d_H(A, A * B) - 0.5| > \epsilon) = 0.$$

Proof. From the Lemma 1, we know that

$$d_H(A, A * B) = \frac{1}{D} \sum_{i=1}^D \mathbb{I}(b_i = -1) = \frac{\text{neg}(B)}{D}.$$

Since B is a random hypervector, each component b_i is drawn i.i.d. from a binary distribution over $\{-1, +1\}$ with equal probability. Again, by the Weak Law of Large Numbers,

$$\lim_{D \rightarrow \infty} \mathbb{P} \left(\left| \frac{\text{neg}(B)}{D} - 0.5 \right| > \epsilon \right) = 0,$$

thus leading to

$$\lim_{D \rightarrow \infty} \mathbb{P} (|d_H(A, A * B) - 0.5| > \epsilon) = 0.$$

□

Proposition 1 (Hamming Distance with sufficiently large D). Let two hypervectors $A, B \in \mathcal{H}^D$ that satisfy

$$d_H(A, B) = \delta,$$

and the random variable Z_i indicates the situation of the i^{th} bit

$$Z_i = \mathbb{I}(a_i \neq b_i).$$

With sufficiently large D , the Z_i can be approximately viewed as an i.i.d. Bernoulli distribution

$$Z_i \sim_{\text{i.i.d.}} \text{Bernoulli}(\delta), \forall i \in \{1, 2, \dots, D\}.$$

Proof. With the definition of Hamming distance, we have

$$\frac{1}{D} \sum_{i=1}^D Z_i = d_H(A, B) = \delta.$$

Observe that this is an empirical mean of $\{Z_i\}$ over D bits. Notice that the Z_i are NOT independent — their sum is fixed to be exactly δD . However, we make the following observations and assumptions to justify such a approximation:

- With sufficiently large D , the possibility of the Hamming distance of A and B completely falls into an arbitrarily small interval around the δ is almost 1

$$\mathbb{P} \left(\left| \frac{1}{D} \sum_{i=1}^D Z_i - \delta \right| > \epsilon \right) \leq 2 \exp(-2D\epsilon^2).$$

- If A and B are generated randomly and conditioned on their Hamming distance being dD , then the mismatch positions mentioned above are uniformly random for every index;

□

To summarize, this proposition provides a new perspective to define the Hamming distance in the large hyperspace. With sufficiently large dimensionality D , Hamming distance between hyper-vectors can be interpreted statistically as the empirical mean of i.i.d. Bernoulli random variables, yielding a probabilistic characterization of similarity.

A.3 THEOREMS

Theorem 1 (Robust to Input Noise). *Let $s^{(1)}, s^{(2)} \in \mathcal{S} \subseteq \mathbb{R}^d$ be two feature vectors. $S = f_{\mathcal{ID}, \mathcal{L}, \Theta}(s)$ denotes the hypervector mapping defined in Equation 2. Suppose that for all indices of the features $n \in \{1, \dots, d\}$,*

$$\frac{|x_n^{(1)} - x_n^{(2)}|}{\Delta_i} \leq \delta,$$

where Δ_i is the difference between the upper and lower bounds of the i^{th} feature value, and $\delta \in [0, 1]$ denotes the maximum distance ratio of the corresponding features. Then, with a sufficiently large D , the expected upper-bound Hamming distance between $S^{(1)} = f_{\mathcal{ID}, \mathcal{L}, \Theta}(s^{(1)})$ and $S^{(2)} = f_{\mathcal{ID}, \mathcal{L}, \Theta}(s^{(2)})$ converges to a monotonically increasing function g with parameter δ

$$\mathbb{E} \left[\sup \left(d_H \left(S^{(1)}, S^{(2)} \right) \right) \right] \rightarrow g(\delta), \quad (22)$$

This implies that the Hamming distance between a sample and its noisy variant is almost surely bounded by $g(\delta)$.

Proof. We consider the $L^{(l_n(x_n^{(1)}))}, L^{(l_n(x_n^{(2)}))}$ first. Since $\frac{|x_i^{(1)} - x_i^{(2)}|}{\Delta_i} \leq \delta$, we can bound the difference of their corresponding Level Hypervectors. By definition 4, we have

$$\begin{aligned} & d_H \left(L^{(l_n(x_i^{(1)}))}, L^{(l_n(x_i^{(2)}))} \right) \\ &= \frac{l_n(x_i^{(1)}) - l_n(x_i^{(2)})}{M-1} \\ &\leq \frac{1}{M-1} \left(\frac{\delta \Delta_i}{\theta_{i,M-1} - \theta_{i,1}} (M-2) + 2 \right) \\ &\leq \frac{M}{M-1} \delta + \frac{2}{M-1} = \delta_d, \end{aligned} \quad (23)$$

With the random flipping performed by $\otimes ID^{(i)}$, $\{L^{(l_n(x_i^{(1/2)}))} \otimes ID^{(i)}\}$ can be viewed as a new set of randomly generated hypervectors, denoted as $\{T^{i(1/2)}\}$, which satisfy the following relationship with Lemma 2

$$\begin{aligned} & d_H \left(T^{i(1)}, T^{i(2)} \right) \\ &= d_H \left(L^{(l_n(x_i^{(1)}))} \otimes ID^{(i)}, L^{(l_n(x_i^{(2)}))} \otimes ID^{(i)} \right) \\ &= d_H \left(L^{(l_n(x_i^{(1)}))}, L^{(l_n(x_i^{(2)}))} \right) \leq \delta_d. \end{aligned} \quad (24)$$

To estimate the upper bound, we treat the inequality as an equality. Furthermore, with Proposition 1, we consider the Hamming distance constraint as a statistically condition, so that for every $T^{i(1)}$ and $T^{i(2)}$ pair, the equality situation at the j^{th} index follows a Bernoulli distribution

$$\mathbb{I} \left(T_j^{i(1)} \neq T_j^{i(2)} \right) \sim_{i.i.d.} \text{Bernoulli}(\delta_d), \forall j \in \{1, 2, \dots, D\}.$$

Next, we consider the situation on the j^{th} index of $S^{(1)} = \bigoplus_{i=1}^d T^{i(1)}$ and $S^{(2)} = \bigoplus_{i=1}^d T^{i(2)}$ as a random variable Z_j that satisfies

$$Z_j = \mathbb{I}(S_{(j)}^{(1)} \neq S_{(j)}^{(2)})$$

Let $p_j^{(1/2)}$ be the number of $+1$ in the $\{T_j^{i(1/2)}\}_{i=\{1,2,\dots,d\}}$, so that the probability of $Z_j = 1$ is

$$P(Z_j = 1) = \sum_{n=0}^d P(Z_j = 1 | p_j^{(1)} = n) \times P(p_j^{(1)} = n).$$

Specifically, by considering the $\{T_j^{i(1)}\}_{i=\{1,2,\dots,d\}}$ follow the i.i.d. Bernoulli(0.5), we have

$$P(p_j^{(1)} = n) = \frac{C_d^n}{2^d}.$$

Consider the situation where $n < \frac{d}{2}$ and d is an odd number to avoid unnecessary complexity, we have the number of $+1$ in the second sample follow a combined Binomial distribution

$$p_j^{(2)}|_{p_j^{(1)}=n} \sim \text{Binomial}(n, 1 - \delta_d) + \text{Binomial}(d - n, \delta_d),$$

Therefore,

$$P(Z_j = 1 | p_j^{(1)} = n) = \sum_{k=\frac{d+1}{2}}^d \sum_{i=\max(0, k-d+n)}^{\min(n, k)} C_n^i \cdot C_{d-n}^{k-i} \cdot \delta^{n+k-2i} (1-\delta)^{d-n-k+2i}.$$

For situation that $n > \frac{d}{2}$, we obtain an entirely analogous result

$$P(Z_j = 1 | p_j^{(1)} = n) = \sum_{k=0}^{\frac{d-1}{2}} \sum_{i=\max(0, k-d+n)}^{\min(n, k)} C_n^i \cdot C_{d-n}^{k-i} \cdot \delta^{n+k-2i} (1-\delta)^{d-n-k+2i}.$$

With the derived results, we can calculate the probability of $P(Z_j = 1)$ as a function of δ_d .

$$g(\delta) = p(\delta_d) = p\left(\frac{M}{M-1}\delta + \frac{2}{M-1}\right) \quad (25)$$

Finally, we consider the average with all the indices make the distribution arbitrarily close to the expectation, which is the probability we just calculated in Eqn. 25, thus complete the proof. \square

This theorem establishes an approximate form of "continuity", showing that the designed mapping ensures that when the input noise is small, the distance between the corresponding mapped outputs is also bounded. In particular, this design exhibits better rejection properties against small perturbations with sufficiently large dimensionality D and relatively large features d .

Theorem 2 (Distance Between Cluster Prototype and Constituents). *Let $S^{(1)}, S^{(2)}, \dots, S^{(N)} \in \mathcal{H}^D$ be independently sampled random hypervectors. Define their sum as $C = [S^{(1)} + S^{(2)} + \dots + S^{(N)}]$. As $D \rightarrow \infty$, for any random hypervector $S^* \in \mathcal{H}^D$, index $j \in \{1, \dots, N\}$, the Hamming distance between C and any component $S^{(n)}$ satisfies*

$$P\left(d_H(C, S^{(n)}) < d_H(C, S^*)\right) \rightarrow 1.$$

Proof. We begin with analyzing the probability that the i^{th} index of C and $S^{(n)}$ is different.

Let $Z_i^{(n)} = \sum_{k \neq n} S_i^{(k)}$, where $S_i^{(k)}$ is the i^{th} value of $S^{(k)}$, so that:

$$C_i = \left[\sum_{k=1}^N S_i^{(k)} \right] = \left[S_i^{(n)} + \sum_{k \neq n} S_i^{(k)} \right] = \left[S_i^{(n)} + Z_i^{(n)} \right].$$

Since the random hypervectors are independently sampled, the $N - 1$ terms $S_i^{(k)}$ ($k \neq n$) are independent random variables satisfying:

$$\mathbb{P}(S_i^{(k)} = +1) = \mathbb{P}(S_i^{(k)} = -1) = 0.5.$$

Since $\frac{S_i^{(k)} + 1}{2} \sim \text{Bernoulli}(0.5)$, their i.i.d. sum $Z_i^{(n)}$ follows a shifted binomial distribution:

$$Z_i^{(n)} \sim 2 * \text{Binomial}(N - 1, 0.5) - (N - 1)$$

Given $S_i^{(n)} = +1$, we have $C_i = [1 + Z_i^{(n)}]$. Without losing generality, we only consider the situation when $N - 1$ is an even number, which lead to

$$P(C_i \neq S_i^{(k)}) = P([1 + Z_i^{(n)}] \neq 1) = P(Z_i^{(n)} < -1) + \frac{1}{2}P(Z_i^{(n)} = -1) = P(Z_i^{(n)} < -1),$$

where $P(Z_i^{(n)} = -1) = 0$ since the sum can only take even values.

With the distribution of $Z_i^{(n)}$, we can further calculate the specific probability:

$$P(C_i \neq S_i^{(n)}) = \frac{1}{2} - 2^{-N} C_{N-1}^{\frac{N-1}{2}}.$$

By symmetry, the same calculation applies if $S_i^{(n)} = -1$. Notice that $\mathbb{I}(C_i \neq S_i^{(n)})$ presents a Bernoulli distribution and this process is independently carried out for every index, we can derive the distribution of the Hamming distance $d_H(C, S^{(n)})$:

$$d_H(C, S^{(n)}) = \frac{1}{D} \sum_{i=1}^D \mathbb{I}(C_i \neq S_i^{(n)}) \sim \frac{1}{D} \text{Binomial}(D, \frac{1}{2} - p(N))$$

where $p(N) = 2^{-N} C_{N-1}^{\frac{N-1}{2}}$.

Due to independently sampling, we can view S^* and B just as two random hypervectors in the hyperspace, so we can apply the result from Lemma 3, we know that

$$d_H(C, S^*) \sim \frac{1}{D} \text{Binomial}(D, \frac{1}{2}).$$

With central limit theorem, these two distributions converge to normal distributions as $D \rightarrow \infty$

$$d_H(C, S^*) \sim \mathcal{N}(\frac{1}{2}, \frac{1}{4}D^{-1}), \quad d_H(C, S^{(n)}) \sim \mathcal{N}(\frac{1}{2} - p(N), (\frac{1}{4} - p^2(N))D^{-1}).$$

Based on that, we have,

$$\begin{aligned} & P(d_H(C, S^{(n)}) - d_H(C, S^*) \geq 0) \\ &= P\left((d_H(C, S^{(n)}) - \frac{1}{2} - \frac{p(N)}{2}) - (d_H(C, S) - \frac{1}{2} - \frac{p(N)}{2}) \geq 0\right) \\ &\leq P\left((d_H(C, S^{(n)}) - \frac{1}{2} - \frac{p(N)}{2}) \geq 0\right) + P\left((d_H(C, S) - \frac{1}{2} - \frac{p(N)}{2}) \leq 0\right) \quad (26) \\ &\leq P\left(\left|d_H(C, S^{(n)}) - \frac{1}{2} - p(N)\right| \geq \frac{p(N)}{2}\right) + P\left(\left|d_H(C, S) - \frac{1}{2}\right| \geq \frac{p(N)}{2}\right) \\ &= 2 * \Phi(-p(N)D^{\frac{1}{2}}) + 2 * \Phi\left(-\frac{p(N)}{\sqrt{1 - 4p^2(N)}}D^{\frac{1}{2}}\right) \end{aligned}$$

we can select appropriate $D = D(p(N))$ to allow the right-hand side of the equation to approach zero arbitrarily by letting $p(N)D^{\frac{1}{2}} \rightarrow \infty$. Thus we have the result

$$P\left(d_H(C, S^{(n)}) < d_H(C, S^*)\right) \rightarrow 1,$$

where Φ is the Cumulative Distribution Function of the standard normal distribution.

Moreover, we further know that the convergence is roughly characterized $\Phi(-p(N)D^{\frac{1}{2}})$.

Notice that $p(N) \rightarrow 0$ as $N \rightarrow \infty$, and the dimension D is required to be dependent on $p(N)$ to make the scale become effective, we apply $N >> D$ for the implementation. Intuitively speaking, we require a sufficiently large N to divide this two normal peak apart given a small $p(N)$.

□

Theorem 3 (Robustness to Hardware Error). *Assume we have a sample hypervector S and two cluster hypervectors C_1 and C_2 , whose initial Hamming distances satisfy:*

$$d_H(S, C_1) = d_1 \quad \text{and} \quad d_H(S, C_2) = d_2,$$

where $d_2 - d_1 = \epsilon > 0$.

We randomly flip a proportion p ($p < 0.5$) of the bits in both C_1 and C_2 , yielding two new hypervectors C'_1 and C'_2 . As $D \rightarrow \infty$, we have

$$P\left(d_H(S, C'_1) < d_H(S, C'_2)\right) \rightarrow 1$$

Proof. Again, we begin with the situation at the i^{th} index. Let X_i and Y_i be the indicator variables denoting whether the i -th bit differs from S after corruption:

$$X_i = \mathbf{1}_{\{(C'_1)_i \neq S_i\}}, \quad Y_i = \mathbf{1}_{\{(C'_2)_i \neq S_i\}},$$

so that the post-corruption Hamming distances are:

$$d_H(S, C'_1) = \frac{1}{D} \sum_{i=1}^D X_i, \quad d_H(S, C'_2) = \frac{1}{D} \sum_{i=1}^D Y_i.$$

Next, we analyze the expectation of each X_i and Y_i . With the view of Proposition 1, with a sufficiently large D , we can transfer the Hamming distance d as a random event with probability d :

- For each i , if C_1 and S originally differ at bit i , which happens with probability d_1 , then flipping that bit with probability p yields:

$$\mathbb{P}(X_i = 1 \mid \text{originally different}) \rightarrow 1 - p, \quad \mathbb{P}(X_i = 0 \mid \text{originally different}) \rightarrow p.$$

- If they originally agree (probability $1 - d_1$), then:

$$\mathbb{P}(X_i = 1 \mid \text{originally same}) \rightarrow p, \quad \mathbb{P}(X_i = 0 \mid \text{originally same}) \rightarrow 1 - p.$$

Hence, the expectation becomes:

$$\mathbb{E}[X_i] \rightarrow d_1(1 - p) + (1 - d_1)p = d_1(1 - 2p) + p.$$

Similarly,

$$\mathbb{E}[Y_i] = d_2(1 - 2p) + p.$$

Since $d_2 = d_1 + \epsilon$ and $1 - 2p > 0$, we have:

$$\mathbb{E}[Y_i] - \mathbb{E}[X_i] = (d_2 - d_1)(1 - 2p) = \epsilon(1 - 2p) > 0.$$

Now define the total difference in post-corruption Hamming distances:

$$Z = \sum_{i=1}^D (Y_i - X_i).$$

Then:

$$\mathbb{E}[Z] = D \cdot (\mathbb{E}[Y_i] - \mathbb{E}[X_i]) = D \cdot \epsilon(1 - 2p).$$

Because X_i, Y_i are bounded, independent random variables, and the variance of each term is bounded, we can apply Hoeffding's inequality to show that:

$$\mathbb{P}(Z < 0) \leq \exp(-cD)$$

for some constant $c > 0$. This implies:

$$\mathbb{P}(d_H(S, C'_1) < d_H(S, C'_2)) = \mathbb{P}(Z > 0) \rightarrow 1 \quad \text{as } D \rightarrow \infty.$$

□